**Article:**
Isner, Jean-Charles Eric Francois, Begum, Afroza, Nuehse, Thomas et al. (2 more authors) (2018) KIN7 kinase regulates the vacuolar TPK1 K+ channel during stomatal closure. Current Biology. 466-472.e4. ISSN: 0960-9822

https://doi.org/10.1016/j.cub.2017.12.046

# KIN7 kinase regulates the vacuolar TPK1 $K^+$ channel during stomatal closure.

AUTHORS: Jean Charles Isner[1], Afroza Begum[2], Thomas Nuehse[3], Alistair M Hetherington[1] and Frans J.M. Maathuis[2]

Affiliations: [1)] School of Biological Sciences, University of Bristol, Life Sciences Building, 24 Tyndall Avenue, Bristol BS8 1TQ, UK,

[2)] Department of Biology, Wentworth Way, University of York, York, YO10 5DD, UK

[3)] Faculty of Life Sciences, Michael Smith Building, Oxford Road, Manchester, M13 9PT, UK

Corresponding author and lead contact: Frans J.M. Maathuis, Department of Biology, University of York, York, YO10 5DD, United Kingdom. Tel: +44-1904-328652, Fax: +44-1904-328505, email: fjm3@york.ac.uk

## Summary

Stomata are leaf pores that regulate $CO_2$ uptake and evapotranspirational water loss. By controlling $CO_2$ uptake stomata impact on photosynthesis and dry matter accumulation. The regulation of evapotranspiration is equally important because it impacts on nutrient accumulation, leaf cooling and enables the plant to limit water loss during drought [1]. Our work centres on stomatal closure [2-6]. This involves loss of potassium from the guard cell by a two-step process. Salt is released across the plasma membrane via anion channels such as SLAC1 [7-9] and depolarisation-activated channels such as GORK [10,11] with the net result that cations and anions exit guard cells. However, this critically depends on $K^+$ release from the vacuole; With ~160 and 100 mM $K^+$ in cytoplasm and vacuole of open guard cells [12], vacuolar $K^+$ efflux is driven by the negative tonoplast potential and this expels $K^+$ from the vacuole via tonoplast $K^+$ channels like TPK1. In all, guard cell salt release leads to a loss of turgor that brings about stomatal closure. First we show that the TPK1 vacuolar $K^+$ channel is important for ABA and $CO_2$-mediated stomatal closure. Next we reveal that during ABA and $CO_2$-mediated closure, TPK1 is phosphorylated and activated by the KIN7 receptor like protein kinase (RLK) which co-expresses in the tonoplast and plasma membrane. The net result is $K^+$ release from the vacuole. Taken together our work reveals new components involved in guard cell signalling and describes a new mechanism potentially involved in fine-tuning ABA and $CO_2$-induced stomatal closure.


## Results and Discussion

The tonoplast located channel AtTPK1 [13,14] was previously shown to affect ABA-induced stomatal closure in *Arabidopsis* [15]. In this investigation we used patch-clamp

electrophysiology to show that GC vacuolar preparations exhibited TPK1 activity (Fig. 1A). Tonoplast channels may show tissue specific properties as was shown for TPC1 [16]. However, single channel conductance and weak voltage dependence of GC TPK1 activity were the same as previously reported for TPK1 currents from mesophyll cell vacuoles [15]. Addition of 0.5 mM Mg-ATP to the cytoplasmic side of the membrane led to a rapid but moderate increase in channel activity. Channel activity was further increased when both Mg-ATP and 14-3-3 protein were present as was shown previously for TPK1 in mesophyll cells [17,18]. On average, ATP alone caused an increase in channel activity that was equivalent to an increase in open time (and therefore current) of ~50% whereas ATP+14-3-3 more than tripled open probability and current (Figure 1B).

The S42 residue forms part of the 14-3-3 binding domain in the TPK1 N-terminus and by using a reconstituted TPK1 N-terminus, Latz, et al. [18] showed that S42 phosphorylation is required for TPK1-14-3-3 interaction. To test if the same residue is responsible for the phosphorylation-dependent changes in GC TPK1 activity, we transiently expressed a mutated (S42A) version of TPK1 in the *tpk1* T-DNA knock out background [15]. The S42A version mimics a constitutively non-phosphorylated form. Normal currents were recorded showing that the channel is fully functional (Figure 1A) but the stimulating effects of both ATP and ATP+14-3-3 were abolished (Figure 1B). Taken together these data show that in GCs TPK1 shows low basal activity, which increases after phosphorylation at S42 and is further elevated after binding of 14-3-3. Figure S1 shows that these characteristics were retained when measuring macroscopic currents.

*ABA causes phosphorylation of TPK1 in planta*

Knowing that ABA induces stomatal closure we decided to test whether TPK1 phosphorylation is ABA-dependent. GC protoplasts were isolated from the *tpk1* mutant that had been transiently transformed with TPK1::YFP (MW 67.7 kD) and were then probed with a phosphoserine specific antibody that recognised the phosphorylated 14-3-3 binding domain [19]. Figure 1C shows a band around 70 kD that increased in intensity after ABA treatment and was absent in the (non-transformed) *tpk1* null mutant. We also tested if ABA increased TPK1 phosphorylation in intact tissue; treating leaves with 40 µM ABA for one hour led to increased TPK1 phosphorylation detected in isolated GC protoplasts (Figure 1D). On the basis of densitometry, 2.5-3-fold higher phosphorylation signals were recorded after ABA treatment (Figure 1E). These data allow us to conclude that phosphorylation of TPK1 is regulated by ABA and opens up the possibility that this is part of the GC ABA signalling network and may be necessary for stomatal closure. It would be interesting to further test this idea using a phosphomimic TPK1 version, for example through substitution of S42 with glutamate. Such genotypes could be evaluated for their transpirational flux, steady state stomatal conductance and responses to various stimuli.

*A receptor like kinase is involved in TPK1 phosphorylation*

To help identify the protein kinase that was responsible for TPK1 phosphorylation we interrogated the SUBA database (http://suba3.plantenergy.uwa.edu.au/) for protein kinases that are annotated as tonoplast-localised. A total of 22 kinase isoforms was found and loss of function mutants were obtained for 16 of these (Table S1). Mutants were tested for an altered channel 'activation response' to ATP and 14-3-3 (Figures S2A and S2B and Data S1). The amount of activation generated by ATP varied but was not significantly different between any of the genotypes (Figure S2B). However, activation by ATP+14-3-3 was significantly ($p<0.001$) lower in the *kin7* mutant compared to that observed in WT.

Furthermore, a role for KIN7 in TPK1 phosphorylation was confirmed by the large reduction in ABA-induced TPK1 phosphorylation in the *kin7* loss of function mutants (Figure 1E).

KIN7 is ubiquitously expressed in all leaf tissues but to investigate whether KIN7 and TPK1 physically interact at the GC tonoplast we employed a BiFC strategy [20,21]. Figure 2A shows an intact and an osmotically ruptured GC protoplast co-transformed with TPK1-$YFP_{Nt}$ and TPK1-$YFP_{Ct}$. As expected, fluorescence is clearly localised in the tonoplast. Similar to the results with TPK1 only, when TPK1-$YFP_{Ct}$ was co-transformed with KIN7-$YFP_{Nt}$ there was a prominent fluorescence signal (Figure 2B, bottom left) in many protoplasts. After osmotic lysis, clear but low intensity fluorescence signal could be observed in the tonoplast of some cells (Figure 2B, bottom right). In contrast, when TPK1-$YFP_{Ct}$ was co-transformed with KIN8-$YFP_{Nt}$ (a kinase very similar to KIN7, see Table S1) no signal was observed in intact or lysed protoplasts (Figure 2C, $n>200$). BiFC experimentation with KIN12, another comparable kinase (Table S1), produced fluorescence signal but never in the tonoplast (Figure S2, $n>200$). These results suggest that TPK1 and KIN7 can directly interact at the tonoplast but that either the incidence is low (see Figure S2), or alternatively, that relatively few proteins are involved.

Apart from electrophysiology and BiFC, we employed a third strategy to probe TPK1-KIN7 interaction. Pull down assays were carried out where the TPK1 N- terminus containing the 14-3-3 domain was used as bait [19] and plant extract derived from shoot tissue expressing KIN7::YFP as prey. Figure S3 shows that, in addition to the BiFC and the electrophysiological data, pull down assays too confirm the interaction between TPK1 and KIN7.

*kin7 and tpk1 are compromised in ABA and $CO_2$-induced stomatal closure*

Previously, we showed that in *tpk1* loss of function mutants ABA-induced stomatal closure is slower than wild type [15] . In the light of our data that TPK1-mediated $K^+$ release is likely to depend on KIN7-mediated TPK1 phosphorylation we compared the kinetics of stomatal closure in wild type, *tpk1* and *kin* loss of function mutants. When ABA-induced stomatal closure was measured in *tpk1* a reduced closing response was observed (Figure 2D) as was previously observed [15]. In two independent mutant alleles of *kin7* delayed ABA-induced closure was also observed. When the *kin7-1* line was rescued with a 35S:*KIN7:YFP* construct, the transformed line reverted to the wildtype phenotype. These results suggest that TPK1 and KIN7 are part of the GC ABA signalling network. This idea is supported by the observation that ABA dependent TPK1 phosphorylation was greatly reduced in both *kin7* mutants (Figure 1E). To investigate whether TPK1 and KIN7 are involved in other stimuli that cause stomatal closure we exposed the WT, *tpk1* and *kin7* mutants to elevated levels of $CO_2$. Figure 2E shows that *tpk1* and *kin7* mutants are markedly unresponsive to 1000 ppm $CO_2$ whether assayed after 3 hours (Figure 2E) or during continuous conductance measurements (Figure S3). These data suggest that TPK1 and KIN7 are also involved in the GC $CO_2$ signalling network.

The latter begs the question whether the KIN7-14-3-3-TPK1 pathway also pertains to other closing stimuli such as the transition from light to dark or a reduction in relative humidity. Preliminary experiments did not show any drought related phenotype in *tpk1* mutants but, since the *tpk1* stomatal phenotype primarily affects closing dynamics rather than the absolute conductance levels [15], more subtle treatments such as alternating relative humidity may be required. Transition to darkness is another stimulus which so far has not been investigated in either the *tpk1* or *kin7* genetic background. Future testing of these

and other closing stimuli should help determine whether the signalling mechanism we describe has more general validity.

*The KIN7 kinase shows dual membrane localisation*

As there are reports that KIN7 is localized to the plasma membrane (SUBA: suba2.plantenergy.uwa.edu.au/) we decided to test whether this protein had a dual membrane localization in GCs. To test this we used KIN7::YFP fusion proteins which were stably expressed under control of the 35S promoter or the endogenous KIN7 promoter. In GC protoplasts derived from transgenic lines, KIN7-YFP was occasionally observed in both plasma membrane and tonoplast (Figure 3A-F). However, in most cases plasma membrane signal greatly predominated (Figure 3C and D) to the extent that the tonoplast signal was only detected after osmotic lysis (Figure 3E and F) when weak but distinct fluorescence can be distinguished in a proportion of cells as was seen in the BiFC experiments. This pattern was consistent for KIN7-YFP expression, irrespective of the promoter driving expression (Figure S4) and clearly point to dual localisation of KIN7. The latter prompted us to investigate whether KIN7 localisation is sensitive to ABA. One half of a KIN7-YFP transformed GC population was treated with 40 µM ABA and subsequently the proportion of protoplasts with tonoplast located signal was determined. Figure 3G shows that the fraction of cells with tonoplast signal more than doubles after exposure to ABA in a time dependent manner. To independently confirm these findings, we carried out Western analyses on tonoplast enriched membrane fractions using the tonoplast aquaporin TIP1;1 as a tonoplast specific marker [22]. Figure 3H shows that initially there is a minimal KIN7 signal in the lower phase of a two phase partitioned membrane prep. However, relative to the tonoplast marker TIP1;1, and within 30 min ABA exposure, the

KIN7 signal is greatly enhanced, to more than 4-fold the initial value (Figure 3I) while similar experiments using high $CO_2$ treatment (1000 ppm, 3h) showed comparable results with an approximately 3-fold increase towards tonoplast expression (Figure S4). These results show that ABA may affect TPK1 activity in less than 30 minutes. Cation flux measurements from Commelina epidermal strips [23] show remarkably similar kinetics of 10-20 minutes between ABA addition and cation release. However, these values are considerably slower than what has been seen for some plasma membrane anion channels. For example, Levshenko et al [24] recorded anion channel activation 1-2 minutes after ABA exposure. There may be several explanations for this difference; Anion channel activation is one of the first responses to ABA and may therefore precede slower cation channel activation. TPK1 activation in intact tissue may be accelerated by unknown cell wall components or, alternatively, different ABA receptors may be involved in the coupling to various membranes.

The above results show that ABA and $CO_2$ treatment led to an increase in tonoplast KIN7 signal. The data do not allow to distinguish whether elevated tonoplast expression was due to *de novo* expression or a consequence of intracellular trafficking. However, preliminary experiments where tissue was treated with cycloheximide (a protein synthesis inhibitor) or chlorpromazine (an endocytosis inhibitor) suggest that tonoplast KIN7 expression was not affected by cycloheximide (Figure S4) but sensitive to chlorpromazine. Such results suggest that endocytosis, rather than de novo protein synthesis, is an essential feature of the shift in KIN7 expression toward the tonoplast.

*Conclusions*

There is a number of conclusions that can be drawn from our work. Our data showing that TPK1 and KIN7 are involved in $CO_2$ and ABA is further evidence that both these closure

signals are able to access a common set of signalling components whose role it is to bring about stomatal closure [25]. In addition to identifying that TPK1 activity is regulated by protein phosphorylation we also report the identity of the regulatory protein kinase. KIN7 has all the hallmarks of an LRR-receptor kinase. It is ubiquitously expressed in many tissues, including mesophyll cells. In addition to GCs, mesophyll cells have been shown to respond to ABA, for example by reducing cell volume (e.g. [26]). This opens the possibility that in mesophyll cells too, KIN7-mediated TPK1 activation plays a role in ABA signalling. Preliminary patch clamp recordings suggest that KIN7 does impact on TPK1 activity in mesophyll cells which supports the above idea but whether this is linked to phosphorylation and 14-3-3 binding of mesophyll cell TPK1 remains to be tested.

Another major questions to emerge from our work is, what is the link between perception of ABA and $CO_2$ on the one hand, and activation of KIN7, binding of 14-3-3 and activation of TPK1 on the other? Upstream signalling components could include well known players such as ABI and OST gene products. Further experimentation with ABA signalling mutants, or ones in $CO_2$ signalling components such as HT1 kinase, RHC1 and RBOH-D/F, will help reveal such interactors. Downstream, 14-3-3 must bring about a conformational change that greatly stimulates channel opening. One mechanism suggests that the TPK1 gate is directly controlled via $Ca^{2+}$ binding to C-terminal EF domains [27] and a model where 14-3-3 sensitises TPK1 $Ca^{2+}$ dependence not only provides a mechanistic explanation but could be tested using electrophysiology.

It is noteworthy that ABA treatment has been reported to result in KIN7 phosphorylation at its C-terminus [28]. If the phosphorylation results in alterations to KIN7 activity this would suggest that at least one additional protein kinase is involved in this signalling network. Our data showing that KIN7 is localized at both the plasma and tonoplast membranes is

supportive of a dynamic, stimulus-induced, mechanism of TPK1 regulation. Inhibition by the endocytotic inhibitor chlorpromazine of the relative shift toward tonoplast expression of KIN7 suggests that the observed increase in KIN7 tonoplast localisation does not originate from de novo KIN7 biosynthesis, but occurs via a hitherto uncharacterised trafficking pathway. Although such findings can only be preliminary and will need further support, retrograde endocytotic trafficking of plasma membrane proteins to endocompartments has been reported: In animals compartmentalisation of receptor kinases generates endosome specific signal transduction complexes [29]. In plants too, trafficking of the steroid receptor kinase BRI1 to endosomal vesicles is believed to be important in intracellular signalling [30].

Control of TPK1 activity through the stimulus-induced localization of KIN7, be it via modulation of expression or via trafficking, represents an attractive mechanism for exerting control over $K^+$ efflux from vacuoles. We have summarised what we know about this pathway in the schema described in Figure 4. What might be the function of this form of regulation? Our phenotypic data showing that mutants in this pathway are distinguished by exhibiting slower rates of closure suggest that this pathway might be in the fine-tuning of stomatal responses rather than switching closure on (or off). However, a better understanding awaits the discovery of additional components in the network.

**ACKNOWLEDGEMENTS:** We thank Bert de Boer (Vrije Universiteit Amsterdam) for his kind gift of 14-3-3 protein and Ingo Dreyer (Universidad de Talca, Chile) for his kind gift of BiFC vectors. We thank Wioletta Pijacka (University of Bristol, UK) for her technical help with Western blotting. AMH and J-C I wish to acknowledge grant support from the UK BBSRC (BB/J002364/1) and the Leverhulme Trust.

**AUTHOR CONTRIBUTIONS**:

JCI and FJM designed research; JCI, FJM, AB and TSN performed research; JCI and FJM analysed data; FJM, AMH and JCI wrote the paper.

## DECLARATION OF INTERESTS

The authors declare no competing interests.

## REFERENCES


1. Hetherington, A.M., and Woodward, F.I. (2003). The role of stomata in sensing and driving environmental change. Nature. *424*, 901-908.
2. Roelfsema, M.R., Levchenko, V., and Hedrich, R. (2004). ABA depolarizes guard cells in intact plants, through a transient activation of R- and S-type anion channels. Plant J. *37*, 578-588.
3. Schroeder, J., Gethyn J Allen, Veronique Hugouvieux, June M Kwak, a., and Waner, D. (2001). Guard cell signal transduction. Annu Rev Plant Physiol Plant Mol Biol. *52*, 627-658.
4. Assmann, S.M., and Jegla, T. (2016) Guard cell sensory systems: recent insights on stomatal responses to light, ABA and CO2. Curr Opinion Plant Biology 33, 157-167.
5. Raghavendra, A.S., Gonugunta, V.K., Christmann, A., and Grill, E. (2010) ABA perception and signalling. Trends in Plant Sciences 15, 395-401.
6. Munemasa, S., Hauser, F., Park, J., Waadt, R., Brandt, B., and Schroeder, J.I. (2015) Mechanisms of ABA-mediated control of stomatal aperture. Current Opinion in Plant Biology 28, 154-162.
7. Geiger, D., Maierhofer, T., AL-Rasheid, K.A.S., Scherzer, S., Mumm, P., Liese, A., Ache, P., Wellmann, C., Marten, I., Grill, E., et al. (2011). Stomatal closure by fast abscisic acid signaling is mediated by the guard cell anion channel SLAH3 and the receptor RCAR1. Sci Signal. *4*, ra32.
8. Geiger, D., Scherzer, S., Mumm, P., Stange, A., Marten, I., Bauer, H., Ache, P., Matschi, S., Liese, A., Al-Rasheid, K.A.S., et al. (2009). Activity of guard cell anion channel SLAC1 is controlled by drought-stress signaling kinase-phosphatase pair. Proc Natl Acad Sci USA. *106*, 21425-21430.
9. Imes, D., Mumm, P., Bohm, J., Al-Rasheid, K.A., Marten, I., Geiger, D., and Hedrich, R. (2013). Open stomata 1 (OST1) kinase controls R-type anion channel QUAC1 in *Arabidopsis* guard cells. Plant J. *74*, 372-382.
10. Ache, P., Becker, D., Ivashikina, N., Dietrich, P., Roelfsema, M.R., Hedrich, R. (2000). GORK, a delayed outward rectifier expressed in guard cells of Arabidopsis thaliana, is a K(+)-selective, K(+)-sensing ion channel. FEBS Lett. *486,* 93-98.
11. Hosy, E., Vavasseur, A., Mouline, K., Dreyer, I., Gaymard, F., Porée, F., Boucherez, J., Lebaudy, A., Bouchez, D., Véry, A.-A., et al. (2003). The *Arabidopsis* outward $K^+$ channel GORK is involved in regulation of stomatal movements and plant transpiration. Proc Natl Acad Sci USA. *100*, 5549-5554.
12. Hills, A., Chen, Z.H., Amtmann, A., Blatt, M.R., Lew, V.L. (2012). OnGuard, a Computational Platform for Quantitative Kinetic Modeling of Guard Cell Physiology. Plant Physiol. 159(3):1026-42.
13. Dunkel, M., Latz, A., Schumacher, K., Muller, T., Becker, D., and Hedrich, R. (2008). Targeting of vacuolar membrane localized members of the TPK channel family. Mol Plant. *1*, 938-949.

14. Voelker, C., Gomez-Porras, J.L., Becker, D., Hamamoto, S., Uozumi, N., Gambale, F., Mueller-Roeber, B., Czempinski, K., and Dreyer, I. (2010). Roles of tandem-pore $K^+$ channels in plants - a puzzle still to be solved. Plant Biol *12 Suppl 1*, 56-63.
15. Gobert, A., Isayenkov, S., Voelker, C., Czempinski, K., and Maathuis, F.J. (2007). The two-pore channel TPK1 gene encodes the vacuolar $K^+$ conductance and plays a role in $K^+$ homeostasis. Proc Natl Acad Sci USA. *104*, 10726-10731.
16. Rienmüller, F., Beyhl, D., Lautner, S., Fromm, J., Al-Rasheid, K.A., Ache, P., Farmer, E.E., Marten, I., Hedrich, R. (2010) Guard cell-specific calcium sensitivity of high density and activity SV/TPC1 channels. Plant Cell Physiol. *51,* 1548-54.
17. Isayenkov, S., Isner, J.C., and Maathuis, F.J. (2011). Rice two-pore $K^+$ channels are expressed in different types of vacuoles. Plant Cell. *23*, 756-768.
18. Latz, A., Becker, D., Hekman, M., Muller, T., Beyhl, D., Marten, I., Eing, C., Fischer, A., Dunkel, M., Bertl, A., et al. (2007). TPK1, a $Ca^{2+}$-regulated *Arabidopsis* vacuole two-pore $K^+$ channel is activated by 14-3-3 proteins. Plant J. *52*, 449-459.
19. Latz, A., Mehlmer, N., Zapf, S., Mueller, T.D., Wurzinger, B., Pfister, B., Csaszar, E., Hedrich, R., Teige, M., and Becker, D. (2013). Salt stress triggers phosphorylation of the *Arabidopsis* vacuolar $K^+$ channel TPK1 by calcium-dependent protein kinases (CDPKs). Mol Plant. *6*, 1274-1289.
20. Waadt, R., Schmidt, L.K., Lohse, M., Hashimoto, K., Bock, R., and Kudla, J. (2008). Multicolor bimolecular fluorescence complementation reveals simultaneous formation of alternative CBL/CIPK complexes in planta. Plant J. *56*, 505-516.
21. Kudla, J., and Bock, R. (2016). Lighting the way to protein-protein interactions: Recommendations on best practices for bimolecular fluorescence complementation analyses. Plant Cell. *28*, 1002-1008.
22. Ludevid, D., Hofte, H., Himelblau, E., and Chrispeels, M.J. (1992). The expression pattern of the tonoplast intrinsic protein gamma-tip in *Arabidopsis thaliana* is correlated with cell enlargement. Plant Physiol. *100*, 1633-1639.
23. MacRobbie EA (2006) Control of volume and turgor in stomatal guard cells. J Membr Biol 210: 131-42
24. Levchenko, V., Konrad, K.R., Dietrich, P., Roelfsema, M.R., Hedrich, R.(2005). Cytosolic abscisic acid activates guard cell anion channels without preceding Ca2+ signals. Proc Natl Acad Sci U S A. 15;102(11):4203-8.
25. Chater, C., Peng, K., Movahedi, M., Dunn, Jessica A., Walker, Heather J., Liang, Y.-K., McLachlan, Deirdre H., Casson, S., Isner, Jean C., Wilson, I., et al. Elevated $CO_2$-induced responses in stomata require ABA and ABA signaling. Curr Biol. *25*, 2709-2716.
26. Kolla, V.A., Suhita, D., Raghavendra, A.S. (2004) Marked changes in volume of mesophyll protoplasts of pea (Pisum sativum) on exposure to growth hormones. J Plant Physiol. *161,* 557-562.
27. Hartley, T.N., Maathuis, F.J.M. (2015) Allelic variation in the vacuolar TPK1 channel affects its calcium dependence. FEBS Lett. *590,* 110-117.
28. Chen, Y., Hoehenwarter, W., and Weckwerth, W. (2010). Comparative analysis of phytohormone-responsive phosphoproteins in *Arabidopsis* thaliana using $TiO_2$-phosphopeptide enrichment and mass accuracy precursor alignment. Plant J. *63*, 1-17.
29. Villaseñor, R., Nonaka, H., Del Conte-Zerial, P., Kalaidzidis, Y., and Zerial, M. (2015). Regulation of EGFR signal transduction by analogue-to-digital conversion in endosomes. eLife. *4*, e06156.
30. Geldner, N., and Robatzek, S. (2008). Plant receptors go endosomal: a moving view on signal transduction. Plant Physiol. *147*, 1565-1574.

31. Schindelin, J., Rueden, C.T., Hiner, M.C., and Eliceiri, K.W. (2015). The ImageJ ecosystem: An open platform for biomedical image analysis. Mol Reprod Dev. 82, 518-529.
32. Pijacka, W., Clifford, B., Tilburgs, C., Joles, J.A., Langley-Evans, S., and McMullen, S. (2015). Protective role of female gender in programmed accelerated renal aging in the rat. Physiol Rep. 3.
33. Hellens, R., Edwards, E.A., Leyland, N., Bean, S., and Mullineaux, P. (2000). pGreen: a versatile and flexible binary Ti vector for *Agrobacterium*-mediated plant transformation. Plant Mol Biol. *42*, 819-832.
34. Pandey, S., Wang, X.Q., Coursol, S.A., and Assmann, S.M. (2002). Preparation and applications of Arabidopsis thaliana guard cell protoplasts. New Phytol. *153*, 517-526.
35. Maathuis, F.J.M., May, S.T., Graham, N.S., Bowen, H.C., Jelitto, T.C., Trimmer, P., Bennett, M.J., Sanders, D., and White, P.J. (1998). Cell marking in *Arabidopsis thaliana* and its application to patch–clamp studies. Plant J. *15*, 843-851.
36. Sinnige, M.P., Roobeek, I., Bunney, T.D., Visser, A.J., Mol, J.N., and de Boer, A.H. (2005). Single amino acid variation in barley 14-3-3 proteins leads to functional isoform specificity in the regulation of nitrate reductase. Plant J. *44*, 1001-1009.
37. Lund, A., and Fuglsang, A.T. (2012). Purification of plant plasma membranes by two-phase partitioning and measurement of $H^+$ pumping. Methods Mol Biol. *913*, 217-223.
38. Rea, P.A., Britten, C.J., and Sarafian, V. (1992). Common identity of substrate binding subunit of vacuolar $H^+$-translocating inorganic pyrophosphatase of higher plant cells. Plant Physiol. *100*, 723-732.

## Figure legends:

### Figure 1: GC TPK1 currents and ABA induced TPK1 phosphorylation.

**(A)** Representative TPK1 currents from one cytoplasmic side out excised patch shows TPK1 currents in control buffer, after addition of MgATP (0.5 mM) or MgATP plus 14-3-3 (100 nM). Mutation of the N-terminal serine 42 to alanine (S42A) leaves channel activity intact but abrogates the effect of ATP and 14-3-3. Currents were recorded at -40 mV and left side arrows indicate closed levels. Amplitude histograms on right show increase in channel openings for wildtype but not S42A. 'Po' open probability quantification based on 60 sec records. **(B)** Normalised relative channel activity, based on open probability data obtained at -80 mV, showing ATP stimulates activity by around 45% and ATP plus 14-3-3 stimulates activity by over 300%, while no significant effect of ATP+14-3-3 is observed for the S42A mutant protein (n=3 independent membrane

patches for each condition, error bars are standard errors.) Data were analysed using one way ANOVA with Tukey post-hoc analysis comparison with control conditions, asterisks denoting $p<0.05$. **(C)** GCs from tpk1 plants were isolated and transiently transformed with TPK1-YFP. Approx 12-16h after transformation half the protoplasts were treated with ABA (1h, 40 µM). Right hand panel: non transformed (NT) protoplasts show complete absence of signal ('T' are transformed protoplasts from the same prep). **(D)** Guard cells isolated from ABA-treated tpk1 loss of function plants, control leaves (WT plants) or ABA treated leaves (WT plants). In (C) and (D), top panels show typical example of blots with antibody against the phosphorylated TPK1 N-terminus. Bottom panels show total protein staining. **(E)** Densitometry based (n=3, bars denote standard errors) fold-changes in TPK1 phosphorylation in control (WT-con) and ABA treated (WT_ABA_L) leaves or protoplasts (WT_ABA_P) and in null mutants of the LRR kinase KIN7 (kin7_ABA). Data were analysed using one way ANOVA with Tukey post-hoc analysis comparison with control conditions, asterisks denoting $p<0.05$. (See also Figures S1 and Table S1).

**Figure 2: Bimolecular fluorescence complementation and loss of function phenotypes in t*pk1* and *kin7*.**

**(A)** Representative image for Arabidopsis GCs cotransformed with $TPK1_{YFP\text{-}Nt}$ plus $TPK1_{YFP\text{-}Ct}$. Note clear vacuolar fluorescence. **(B)** GC protoplasts expressing $KIN7_{YFP\text{-}Nt}$ plus $TPK1_{YFP\text{-}Ct}$ . Note clear signal in the tonoplast. **(C)** GC protoplast expressing $KIN8_{YFP\text{-}Nt}$ plus $TPK1_{YFP\text{-}Ct}$. Note the absence of any fluorescence signal. In all cases, top two panels show DIG images of intact and osmotically ruptured protoplast (releasing the large central vacuole). Bottom panels show corresponding YFP fluorescence signal. Scale bar is 5 µm. **(D)** Leaves of wild type (WT), TPK1 and KIN7 loss of function mutants

KIN7 complemented plants were exposed to 100, 10 or 1 µM ABA and start ('Control') and end (30 minute ABA exposure) conductance values were recorded. **(E)** Stomata were opened by exposure of leaves to 400 ppm $CO_2$ for 2 hours. Subsequently, peels were either aerated with 1000 ppm [$CO_2$] or continued to be aerated with 400 ppm [$CO_2$]. Three hours later, stomatal apertures were measured. Data in D and E were analysed for significance using a one way ANOVA with Tukey post-hoc analysis. Asterisk denotes $p<0.05$. (See also Figures S2 and S3).

**Figure 3: KIN7:YFP expression patterns.**

**(A)** DIC image of intact Arabidopsis GC transformed with KIN7:YFP. **(B)** Corresponding fluorescence image showing expression in both plasma membrane and tonoplast (arrows). **(C and D)** DIC and fluorescence image of GC protoplast showing prominent expression in the plasma membrane only. **(E)** DIC image of osmotically ruptured protoplast releasing the large vacuole**. (F)** Corresponding fluorescence image showing weak but distinct tonoplast expression. **(G)** The proportion of lysed guard cell protoplasts that shows tonoplast KIN7 expression increases after ABA treatment. **(H)** Western immunoblot showing increasing level of KIN7-GFP expression in response to ABA. The vacuole specific aquaporin TIP1;1 was used as tonoplast marker whereas the lack of cross reactivity with the $H^+$-ATPase AHA1 (a plasma membrane specific marker) in the 'lower phase' (LP) shows absence of plasma membrane. 'MF': microsomal fraction showing positive reactivity for all three probes. **(I)** Quantification based on densitometry measurements (using ImageJ) of relative increase in KIN7 expression in the tonoplast. Scale bar in A-F is 7 µm. Data depicted in G and I are based on 3 or more independent experiments, bars denote standard errors and data were analysed using

one way ANOVA with Tukey post-hoc analysis comparison with control conditions. Asterisk denotes $p<0.05$. (See also Figure S4).

**Figure 4: A model for coupling ABA and TPK1.**

ABA perception leads to activation of the LRR kinase KIN7. Increased tonoplast expression of KIN7 and/or KIN7 traffic from plasma membrane (PM) to tonoplast (TO) brings KIN7 in the vicinity of TPK1. At the tonoplast, phosphorylation of S42 in the N-terminal 14-3-3 binding domain allows 14-3-3 binding to TPK1, which leads to drastically increased TPK1 activity and stomatal closure.

## METHODS

## CONTACT FOR REAGENT AND RESOURCE SHARING

Further information and requests for resources and reagents should be directed to and will be fulfilled by the Lead Contact, Frans Maathuis (frans.maathuis@york.ac.uk)

## EXPERIMENTAL MODEL AND SUBJECT DETAILS

**Plant material and growth.** *Arabidopsis thaliana* (L) ecotype Columbia (0) wild type, *tpk1* (SALK line 146903; [15] and kinase mutants and kinase mutants obtained from NASC (see Table S1).

## METHOD DETAILS

### Plants

*Arabidopsis thaliana* (L) ecotype Columbia (0) wild type, *tpk1* and kinase mutants were grown for 3 to 4 weeks in soil (F2, Levington, UK) at 18/22°C night/day temperature in a glasshouse with day lengths of 14 h, supplemented with artificial light of around 200 µmol $m^{-2}$ $sec^{-1}$ as described [17]. T-DNA insertion lines for kinase mutants and the forward and reverse primers that were used to test for homozygosity and transcript can be found in Table S1 and S2.

### Cloning of kinases in the BiFC vector

KIN8 and KIN12 were cloned from cDNA produced from total RNA: Total RNA was extracted from *Arabidopsis* leaves with RNeasy Plant Mini Kit (Qiagen GmbH, Germany). First strand cDNA

was synthesised using SuperScript II Reverse Transcriptase kit (Life Technologies Ltd, UK) with the following primers: kin8bifcfwd and kin8bifcrev, kin12bifcfwd and kin12bifcrev (Table S2). KIN8 and KIN12 fragments were amplified using kin8bifcfwd+kin8bifcrev and kin12bifcfwd+ kin12bifcrev primers respectively (Table S2). KIN7 was PCR-amplified from the full length cDNA clone U12357 (http://abrc.osu.edu/) using the kin7bifcfwd and kin7bifcrev primers (Table S2). Amplified fragments were digested using SpeI and XhoI for KIN7 and KIN8 or BamHI and XhoI for KIN12 and inserted in pSPYNE [20].

**Quantification of BiFC signals**

To be able to compare BiFC signals from various combinations, ImageJ software [31]) was used to measure signal intensity from the vacuolar and plasma membranes. Values were corrected by subtracting signal intensity from nearby background. Signal from TPK1_YFP_Nt+TPK1_YFP_Ct (which forms a dimer) was used as positive control and the signal from kin12_YFP_Nt+TPK1_YFP_Ct (which shows signal in ER and PM but not, or extremely little, in the tonoplast) used as negative control. Quantitative data for BiFC fluorescence signal are shown in Figure S2.

**TPK1 pull-down assay**

Pull-down assays were used to confirm the interaction between the N-terminus part of TPK1 and KIN7. The sequence corresponding to the first 81 amino acids of TPK1 (NTPK1) was amplified by PCR using tpk1bamhIf and tpk1xhoir primers (Table S2) and cloned into the pGEX6P-1 vector (GE Healthcare, Amersham, UK). GST and GST::NTPK1 expression was induced in 1l culture of *E. coli* BL21 at 37°C with 1mM IPTG for 4 hours. Cells were collected and lysed in PBS-T buffer (PBS pH 7.3, 0.1% Trion X-100) by sonication. After centrifugation, the lysate was cleared using 0.45 µm filters. GST or GST::NTPK1 was bound to 500 µl of Glutathione Sepharose 4B (GE Healthcare, Amersham, UK) for 2h. 50 µl bead aliquots washed with buffer P (HEPES 50mM pH7.3, 2mM CaCl2, 2mM MgCl2, 2mM KCl, 100mM NaCl, 1% CHAPS) and protease inhibitor cocktail IV (Calbiochem, Merck, Feltham, UK) were incubated overnight with either proteins extracted with buffer P from plants expressing wild type KIN7 or KIN7::YFP. The next day, beads were washed 4 times with the same buffer. Bound proteins were eluted with SDS–PAGE Protein Sample Buffer (2×) and loaded on a 10% acrylamide gel. Western blotting was performed as described previously [32]. Rabbit anti-GFP (Thermofisher, Paisley, UK) and swine anti-rabbit Immunoglobulins HRP (Agilent, Stockport, UK) were used and the resulting signal in the presence

of Luminata Forte substrate (Merck, Feltham, UK) was imaged with Fusion Pulse imaging system (Vilber Lourmat, Marne-la-Vallée, France).

**Cloning of KIN7:YFP and *Arabidopsis* plant transformation**

KIN7 was PCR amplified from the clone U12357 (http://abrc.osu.edu/) with the kin7yfpfwd and kin7yfprev primers (Table S2) and inserted in the pART7 vector [33]. The NotI fragment containing the 35S:KIN7:YFP fragment was subsequently inserted in pGREEN0229. *Arabidopsis* plants were transformed by floral spraying as described in [33]. Briefly, *Agrobacterium* was grown in 50 mL liquid YEB medium for two days or until the OD reached 3. The cells were spun down (5 min, 4000*g*) and resuspended in 20 mL of 0.1x MS medium, 5% sugar, 0.1% Silwet L-77, pH 5.7. Every two weeks, flowering plants were sprayed with *Agrobacterium* using an airbrush. For pKin7::KIN7:YFP, 589bp upstream of the ATG was amplified from genomic DNA with promkin7fwd and promkin7rev primer (Table S2). This Fragment was inserted in the 35S::KIN7::YFP vector instead of the 35S promoter, which was removed using StuI and XhoI.

**Protoplast isolation:**

Guard cell protoplasts were isolated as described by Pandey, et al. [34]. 40 fully expanded leaves were blended in water for 1 minute using a waring SS515 Blender (Cole-Parmer UK) and poured onto a 200 µM mesh to collect epidermes. Epidermes were incubated in 45% $H_2O$, 55% basic solution (0.5 mM $CaCl_2$, 0.5mM $MgCl_2$, 0.01 mM $KH_2PO_4$, 0.5 mM ascorbic acid, 550 mM sorbitol, 0.2% BSA, 0.7% cellulysin, 5 mM MES/Tris pH 5.5) for 1.5 h at 30°C. The epidermes were then incubated in basic solution supplemented with cellulase Onozuka RS 0.01% and pectolyase Y23 for 1 h at 30°C. Guard cell protoplasts were collected after passing the solution through a 20 µm mesh.

Mesophyll protoplast were extracted from Arabidopsis leaves according to {Isayenkov, 2011 #4}. Leaves were cut in 1-mm sections and digested for 4 h in an enzyme solution containing 1.5% cellulose RS, 0.75% macerozyme, 0.6 m mannitol, 10 mm 2-(N-morpholine)-ethanesulphonic acid (MES), pH 5.6 and 1 mM $CaCl_2$, in which proteases were heat inactivated for 10 min at 55°C. Protoplasts were filtered and centrifuged for 3 min at 500 g and resuspended in protoplast incubation solution (0.6 M mannitol, 4 mM MES, pH 5.7, 4 mM KCl and 3 mm $CaCl_2$)

**Electrophysiology**

Vacuole release, equipment and analyses were as described in Maathuis, et al. [35]. After transfer of protoplasts to the recording chamber, vacuoles were released by washing protoplasts with a

solution containing 10 mM EDTA, 10 mM EGTA, pH 8 with an osmolarity of 350 mOsM. Standard experimental solutions for bath and pipette contained 100 mM KCl, 0.1 mM $CaCl_2$, 5 mM MES/Tris pH 7 and sorbitol adjusted to 430 mOsm total osmolarity. Open probability (Po) was calculated as described in Gobert, et al. [15] and defined as: Po = (t_open/t_total)/n where 'n' is an estimate of the number of channels in the membrane patch derived from the maximum number of open levels observed in the recording. Recordings of 60 s duration (t_total) at a membrane potential of -80 mV were analysed by using a 50% threshold technique to define current transitions and calculate t_open to determine Po. Open probability data were obtained from 3 to 10 individual protoplasts (see Figure S2 and Data S1). To compare different genotypes, the increase in Po in response to ATP and ATP+14-3-3 was calculated for each experiment and 'fold changes' were subsequently averaged across experiments. ATP was added as Mg-ATP at a final concentration of 0.5 mM. 14-3-3 protein (as Hv14-3-3B or Hv14-3-3C; GenBank accessions X93170 and Y14200 respectively [36] was a kind gift from Bert de Boer (Vrije Universiteit, Amsterdam) and added to a final concentration of 0.2µg/ml.

**Imaging**

Intact and osmotically disrupted guard cells were photographed on a Zeiss epifluorescence microscope using bright light, DIC or epifluorescence (465-495 nm excitation and 515 nm emission wavelength) with a 20x, 40x or 63x objective. Confocal imaging was performed using a Zeiss LSM510 Meta microscope (Carl Zeiss, http://www.zeiss.com).

**Leaf Stomatal conductance and apertures**

To record responses to ABA, leaves of mature plants were removed at approx 10:00h and incubated in 'opening' buffer (10 mM KCl, 10 mM MES-KOH pH 6.15) for 2 h in the light to induce maximum opening. Subsequently, $H_2O$ gas exchange was determined (in the same buffer) using an infrared gas analyser, Li-Cor 6400 (LI-COR, Cambridge, UK) to obtain a starting conductance value. Subsequent values were obtained after 30 min incubation in control (no ABA) or ABA (1, 10 or 100 µM final concentration) buffer. Each experiment was carried out using three leaves and in total 12-24 leaves from 3-4 individual plants were used for each treatment. Changes recorded in control treatments (no ABA) were subtracted from those obtained from ABA treated leaves.

To obtain time courses for the response to elevated [$CO_2$], stomatal conductance was measured using infrared gas analysis. Measurements were performed using a portable photosynthesis system attached to a leaf chamber with a 2.5 $cm^2$ leaf area (Walz GFS-3000). $CO_2$ was scrubbed from

external air using soda lime and resupplied from a liquid $CO_2$ cartridge to maintain $CO_2$ concentrations of either 400 or 1000 ppm. Temperature was maintained at 22°C and the absolute humidity to 16000 ppm to obtain a relative humidity of 64.5%. Air flow was 400 $\mu mol.s^{-1}$, light intensity was 120 $\mu mol.m^{-2}\ s^{-1}$. For each measurement, an individual mature leaf was placed in the leaf chamber, while still attached to the plant. Leaves were left in the chamber for 30 min before measurements were taken to allow them to acclimatise to chamber conditions and for gas exchange to stabilise. Measurements were then logged every 10 secs and averaged every 2.5 min. Data represent the mean +-SEM from 3 different plants.

To obtain stomatal apertures, leaf epidermes were removed from fully expanded leaves of 5 to 6 week old plants. They were collected cuticle-side up on $CO_2$-free 10 mM MES/KOH (pH 6.15) in 5cm Petri dishes (Sterilin, UK) at 22°C for 30min. Epidermal peels were transferred to fresh Petri dishes and incubated in the light under a fluence rate of 120 $\mu mol.m^{-2}.\ s^{-1}$ in 50mM KCl, 10 mM MES/KOH (pH 6.15) at 22°C 2 hours whilst being aerated with an air stream containing 400 ppm [$CO_2$] from a pressurised cylinder (BOC, Special Gasses, UK) by bubbling directly into the buffer. Subsequently, peels were either aerated with 1000ppm [$CO_2$] or continued to be aerated with 400ppm [$CO_2$]. After 3h, peels were removed, mounted on slides and measurements of stomatal aperture were recorded using an inverted microscope (Leica DM-IRB, Leica UK). Forty stomatal pores were measured per treatment in three separate replicated experiments (total stomatal number = 120; n = 3). To avoid bias, experiments were performed without knowing the identity of the plants and the treatments until data were collected. Data were analysed using one-way ANOVA.

**Immunoblotting**

Guard cell protoplast preparations were visually inspected and only used when containing fewer than 1% mesophyll protoplasts. ABA treatment (40 µM, 1 hour) was either done on intact leaves in buffer (containing 20 mM KCl, 10 mM MES/KOH pH 6.1) at ~150 $\mu mol.s^{-1}.m^{-2}$ light, or on isolated protoplasts in buffer (containing 500 mM Sorbitol, 10 mM KCl, 1 mM $CaCl_2$, 10 mM MES/Tris pH 5.5). In the latter case, protoplasts were isolated from *tpk1* mutants, and transiently transformed with pART7:TPK1:YFP [15]. Around 16h after transformation, protoplasts were divided in two population with one exposed to ABA (conditions as above). After treatment, protoplasts were resuspended in 'RIPA' buffer (1% Triton X 100, 0.1% SDS, 100 mM NaCl, 10 mM $Na_2HPO_4$ and 10 mM $NaH_2PO_4$, pH 7.2 plus protease inhibitor cocktail 'cOmplete EDTA free' from Roche UK) and stored at -20°C.

For analysis of phosphorylation levels, protein samples (40µg) were precipitated by methanol-chloroform extraction, separated by SDS-10% acrylamide gel electrophoresis and transferred onto nitrocellulose (Hybond-ECL, GE Healthcare). Prior to blocking (5% BSA, TBS), protein levels were visualised with Ponceau S (0.1% w/v in 1% Acetic acid). TPK1 phosphorylation was detected by immunoblotting overnight with anti-pBAD-Ser136 (1:200, i.e. 75 µL in 15 ml, rabbit polyclonal serum, Santa Cruz sc-12969; secondary antibody IRDye 800CW Donkey anti-rabbit, LI-COR 926-32213) and visualised by infrared fluorescence (ODYSSEY CLx, LI-COR). Average phosphorylation signal was calculated using densitometry (ImageJ v 1.48).

**Isolation of tonoplasts and Western blotting**

Five plants at the rosette stage were coated using a paint brush with tween 0.05%, cycloheximide (CHX) 50 µM or chlorpromazine (CPZ) 50 µM in tween 0.05%, one hour before being sprayed with ABA (100 µM) or with a mock solution (tween 0.05%). One hour after ABA treatment, the samples were frozen in liquid nitrogen and ground using a mortar and a pestle. Microsomes were extracted according to Lund and Fuglsang [37] with an altered homogenisation buffer according to Rea, et al. [38]. Briefly, ground material was extracted in 1.1 M glycerol, 5 mM Tris-EDTA, 5 mM DTT, 1% [w/v] PVP-40, 1 mM PMSF, 70 mM Tris-Mes [pH 8.0]) and centrifuged at 6,000g for 10 min. The pellet was resuspended in 3.5 mL buffer 330/5 (0.33 M sucrose, 5 mM potassium phosphate pH 7.8) using a glass homogenizer. Three grams of microsomal fraction was added on top of 9 g polymer solution (3.72 g of 20% Dextran T500 solution, 1.86 g of 40% PEG4000 solution, 1.08 g sucrose, 225 µL potassium phosphate buffer 0.2 M pH 7.8, 18 µL KCl 2 M, $H_2O$ up to 9 g). In parallel, a blank tube was made with 3 g of buffer 330/5 that was added on top of the polymer solution. The tubes were gently inverted 12 times and centrifuged at 1,000*g* for 5 min. The lower phase enriched in tonoplast was collected and re-purified using the top phase of the blank tube. The bottom phase was collected and diluted 10 times with buffer 300/5. The tonoplasts were centrifuged at 100,000*g* for 60 min. The lower phase enriched in tonoplast was resuspended in 0.1 ml RIPA buffer (Fisher scientific, Nottingham, UK) and loaded onto a 4-12% SDS-PAGE NuPAGE™ (Thermofisher, UK). The western blotting was performed according to Pijacka, et al. [32]. Briefly, an Amersham ECL Plex Western blotting system was used on which the gel was run for 2 hours at 120V and protein was subsequently transferred onto a low-fluorescent PVDF membrane (GE Healthcare, Buckinghamshire, UK) using NuPAGE Transfer Buffer (Thermofisher, UK) for 1 hour at 30V in a mini gel tank (Thermofisher, UK). The membrane was cut horizontally in two parts,

589 with the upper part incubated overnight at 4°C with anti-GFP antibody (at 1:2000 dilution) and the
590 bottom part with anti TIP1-1 antibody (at 1:5000 dilution), ensuring equal protein ratio between
591 lanes. Fluorescent secondary antibodies were incubated for one hour and the blots were imaged
592 using fluorescent laser scanner (Typhoon, GE Healthcare, Buckinghamshire, UK). Quantification
593 of bands was performed using CLIQS software (Totallab, Newcastle upon Tyne, UK).
594 To determine change in tonoplast expression in response to ABA or $CO_2$, plants were treated for up
595 to 2h with 50 µM ABA or 1000 ppm $CO_2$. Immunoblotting was carried out as described above and
596 relative expression levels were determined using TIP1;1 as marker and ImageJ [31] software to
597 quantify band intensities.
598 **QUANTIFICATION AND STATISTICAL ANALYSIS**
599 Where statistical testing of data was applied, it is indicated in the legend of the respective figure, as
600 is the number ('n') of experimental replicates. For ANOVA analyses, Prism 6 (Graphpad software)
601 was used. If ANOVA revealed significant ($p < 0.05$) effect of group, post hoc test used to determine
602 p values for all relevant comparisons is mentioned in the figure legends.
603 **Data S1 'Patch clamp open probabilities' (related to Figures 1E and S2A).** The spreadsheet
604 shows open probabilities for each kinase genotype in control, plus ATP or plus ATP+14-3-3
605 conditions.

Figure1

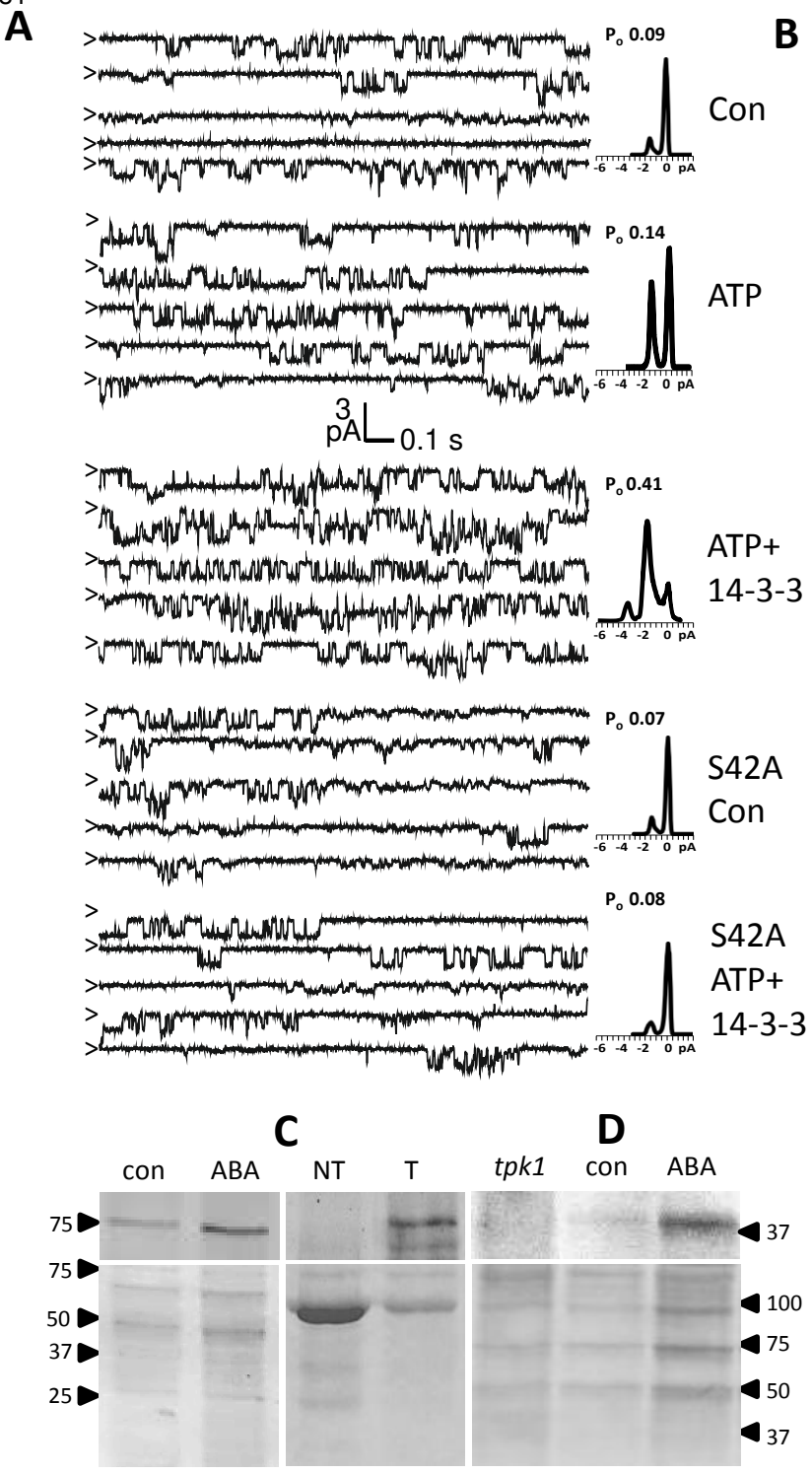
A
Po 0.09
Con
Po 0.14
ATP
3 pA
0.1 s
Po 0.41
ATP+
14-3-3
Po 0.07
S42A
Con
Po 0.08
S42A
ATP+
14-3-3
-6 -4 -2 0 pA

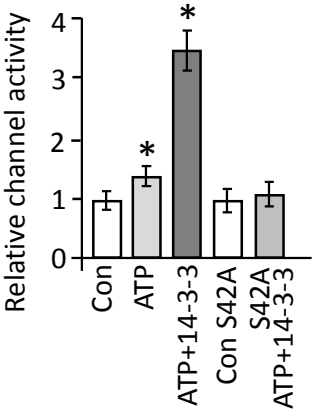
B
Relative channel activity
0
1
2
3
4
*
*
Con
ATP
ATP+14-3-3
Con S42A
S42A
ATP+14-3-3


C
con
ABA
NT
T
75
75
50
37
25
D
tpk1
con
ABA
37
100
75
50
37

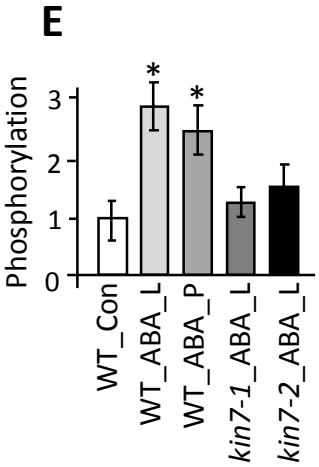
E
Phosphorylation
0
1
2
3
*
*
WT_Con
WT_ABA_L
WT_ABA_P
kin7-1_ABA_L
kin7-2_ABA_L

Figure2

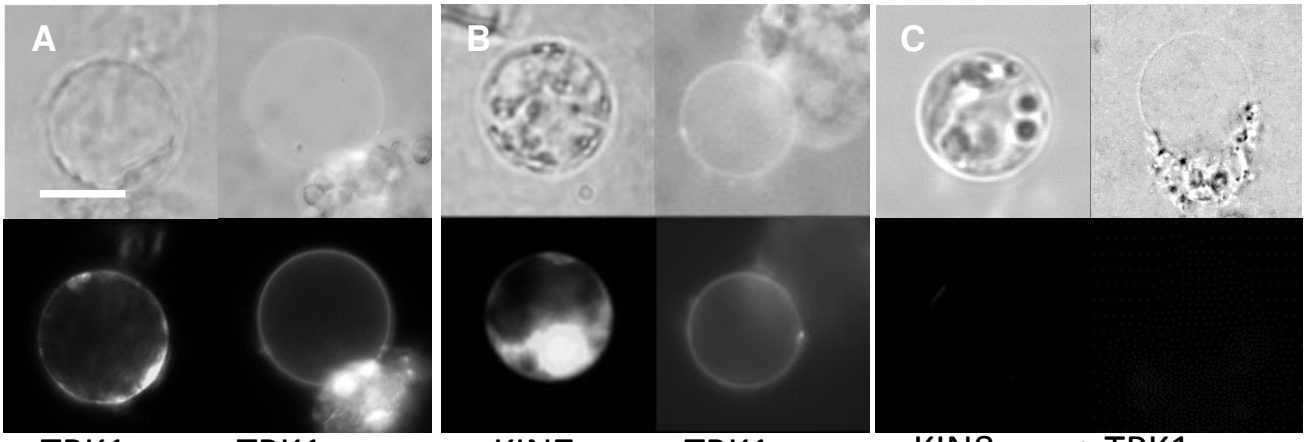
A
B
C
TPK1YFP-Nt+ TPK1YFP-Ct
KIN7YFP-Nt+ TPK1YFP-Ct
KIN8YFP-Nt+ TPK1YFP-Ct

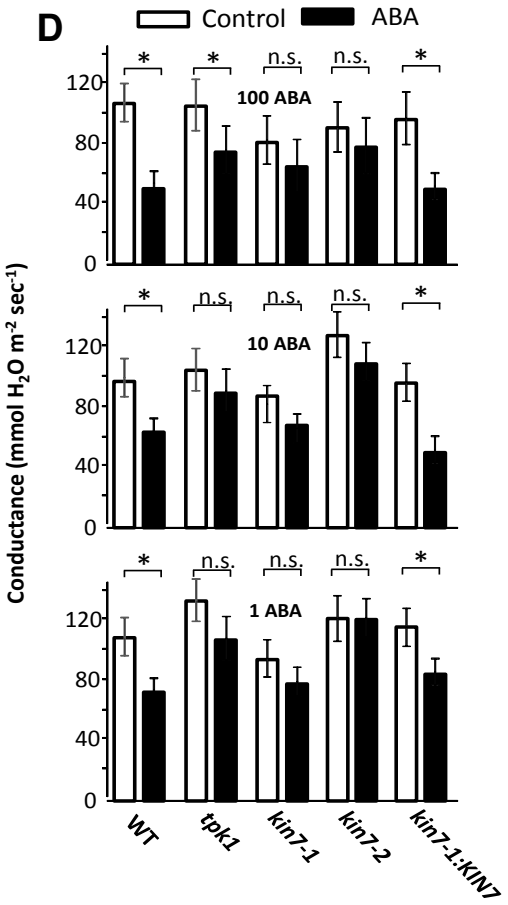
D
Control
ABA
100 ABA
10 ABA
1 ABA
Conductance (mmol H2O m-2 sec-1)
WT
tpk1
kin7-1
kin7-2
kin7-1:KIN7

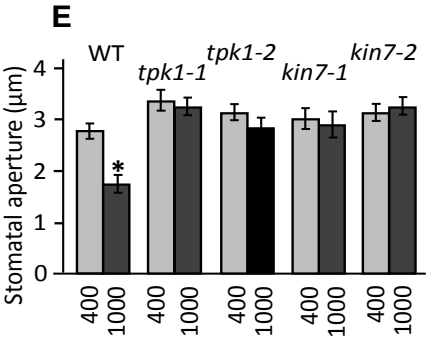
E
WT
tpk1-1
tpk1-2
kin7-1
kin7-2
Stomatal aperture (µm)
400
1000

Figure3

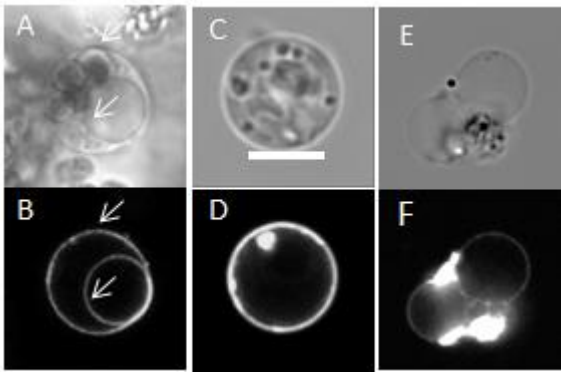
A
C
E
B
D
F

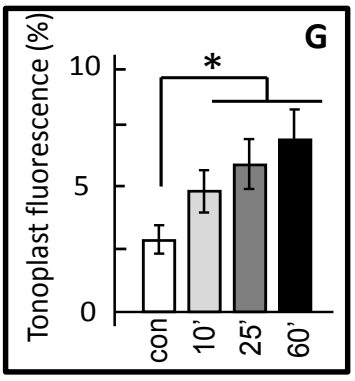
G
Tonoplast fluorescence (%)
10
5
0
*
con
10'
25'
60'

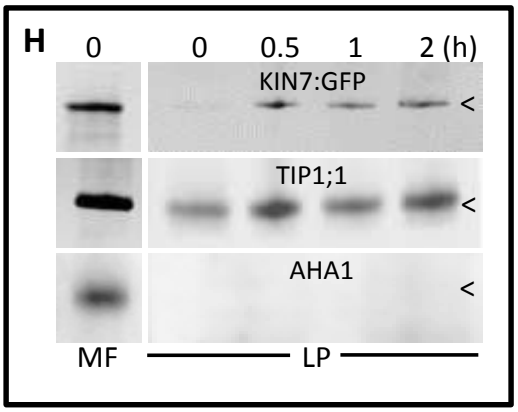
H
0
0
0.5
1
2 (h)
KIN7:GFP
TIP1;1
AHA1
MF
LP

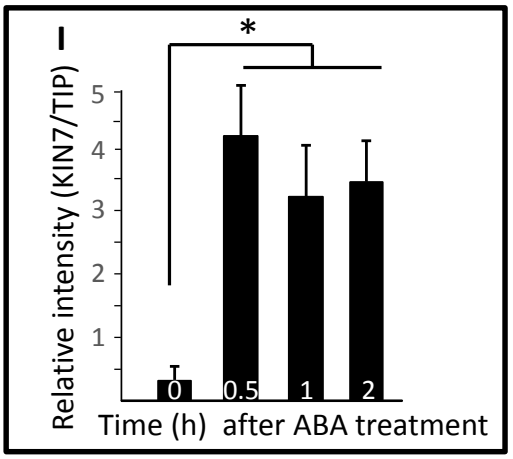
I
*
Relative intensity (KIN7/TIP)
5
4
3
2
1
0
0.5
1
2
Time (h) after ABA treatment

Figure4

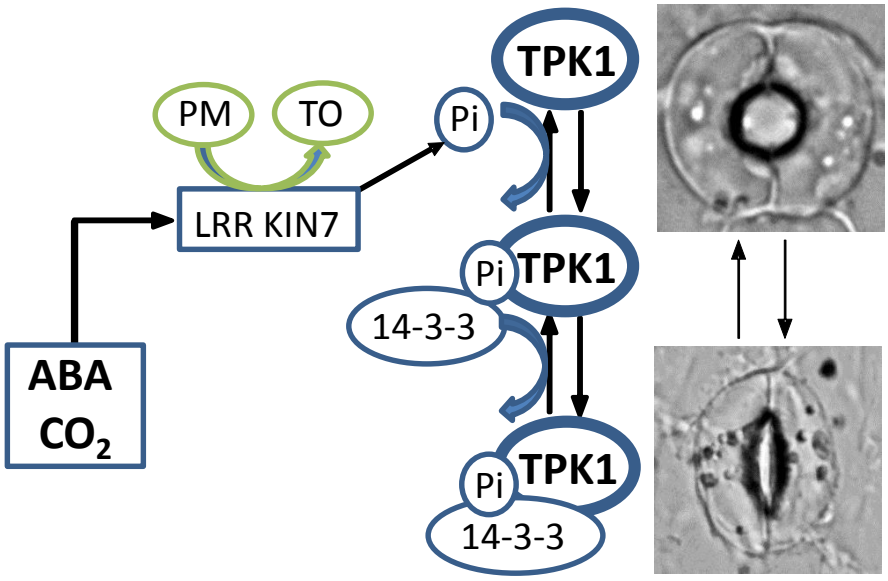

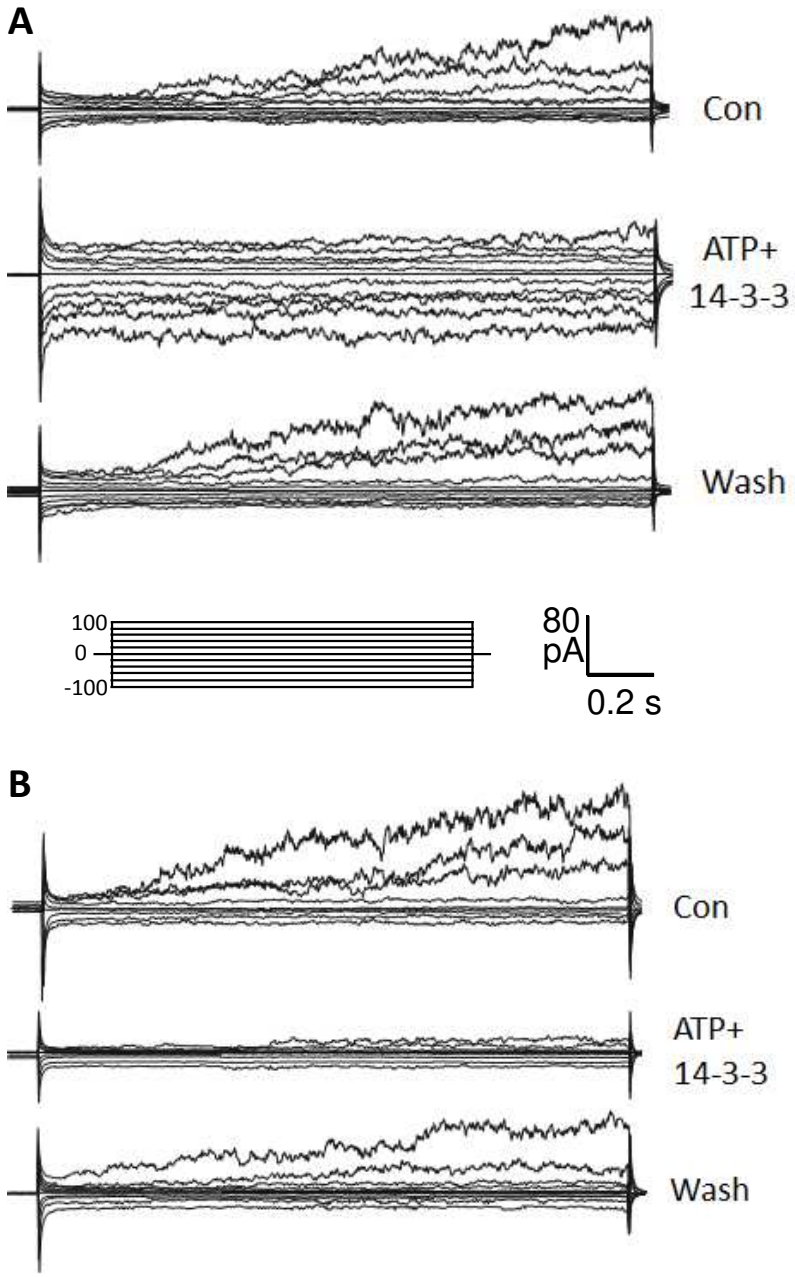


**Figure S1: Whole vacuole currents (relating to Figure 1).**
**(A),** WT guard cell whole vacuole currents in standard buffer, after exposure to buffer containing ATP+14-3-3 and after washout of ATP and 14-3-3. **(B)** Same protocol as shown in (A) for a vacuole that expresses TPK1 with the S42A mutation. Note voltage dependent activation of the SV-type current at positive voltages in control conditions and its inhibition by 14-3-3. Also note absence of TPK1 current activation in the S42A mutant. Inset shows applied voltage clamp protocol (-100 to 100 mV).

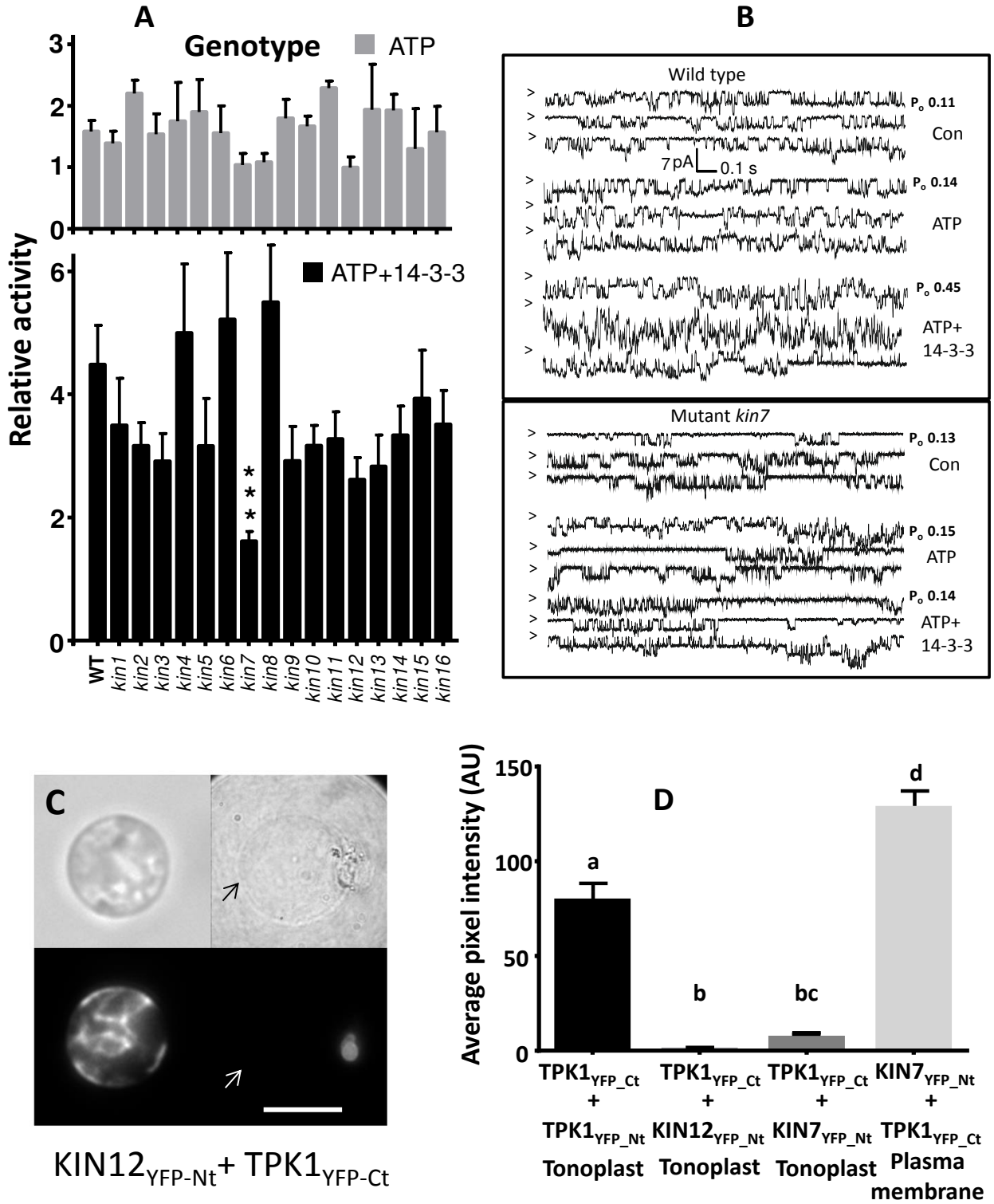


**Figure S2: Kin mutant currents and BiFC (relating to Figure 2).**
**(A)** Vacuolar cytoplasmic side out patches (n=5 to 10), isolated from wild type plants and from 16 different kinase loss of function mutants were recorded in control buffer, in the presence of MgATP, and MgATP plus 14-3-3 protein. Channel activity in the presence of ATP (or ATP+14-3-3) was compared to that measured in the control solution. The ratios of activities between ATP (or ATP+14-3-3) and control solution were then used for analysis. Data show the average for each genotype +/- SEM. The *kin7* genotype stimulatory effect of 14-3-3 (bottom panel) was significantly lowered compared to the WT. Data were tested using

a one-way ANOVA with Dunnett post hoc test analysis ***p<0.001. **(B)** Example traces that reflect the different levels of current stimulation by ATP and by ATP+14-3-3 for wild type, and *kin7* KO mutants. **(C)** BiFC fluorescence in guard cell cotransformed with $KIN12_{YFP\text{-}Nt}$ and $TPK1_{YFP\text{-}CT}$. Top two panels show DIC images of intact and osmotically ruptured protoplast. Bottom panels show corresponding fluorescence signal. Scale bar is 10 µm. **(D)** Quantification of BiFC fluorescence signals. Data were analysed using one way ANOVA with Tukey post-hoc analysis, different letters denoting p<0.05.

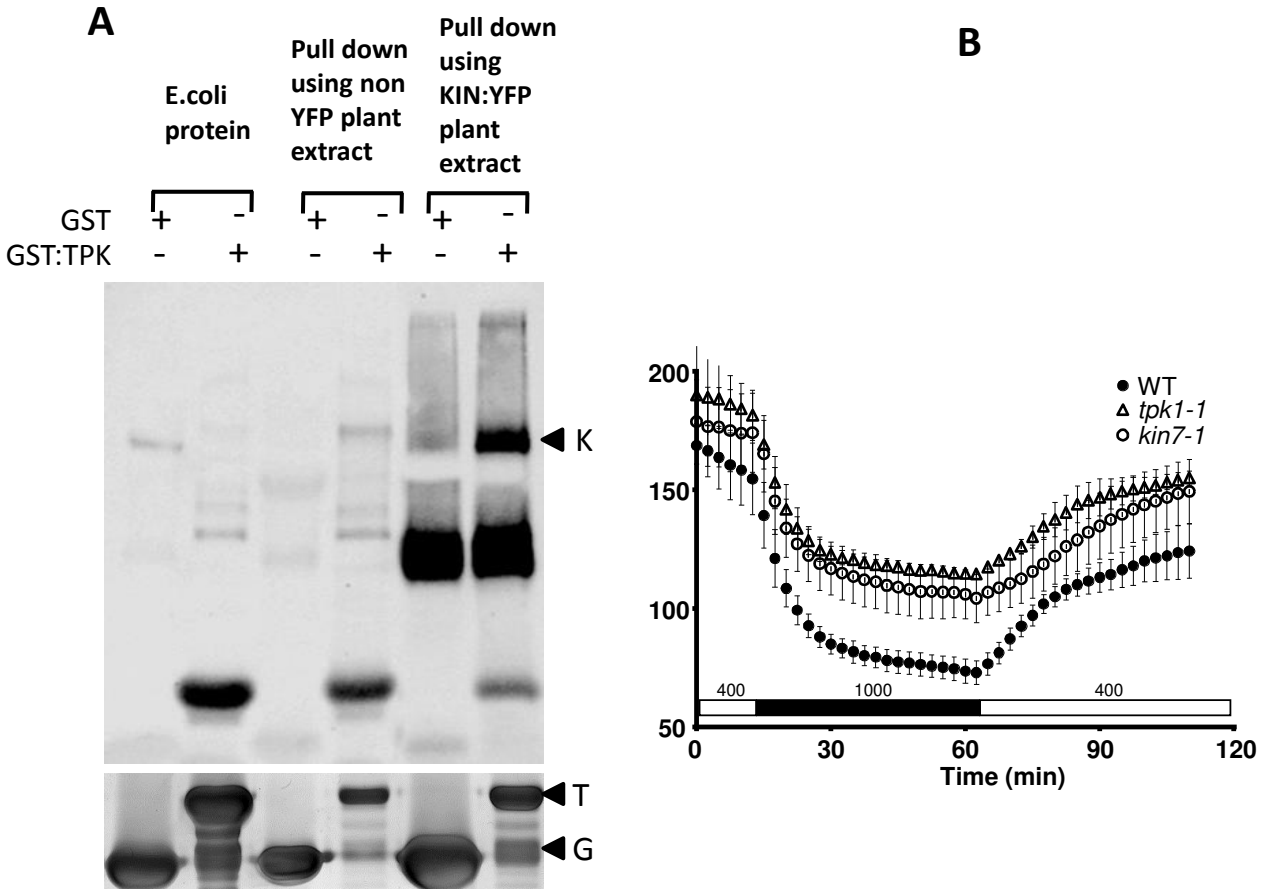


**Figure S3: Pull-down assays and stomatal conductance in response to elevated $CO_2$ (relating to Figure 2).**

**(A)** Pull down assays were carried out using the N-terminal part of TPK1 fused to GST as bait (or GST alone) and leaf extract from wild type plants or plants expressing KIN7::YFP as bait. A primary anti-GFP antibody and HRP-coupled secondary antibody were used to visualise bands on the blot. Arrow head on the top panel (K) depicts 100 kDa (expected KIN7::YFP size ~95 kDa), bottom panel G for GST (~26 kDa) and T for GST:TPK1 (~37 kDa). The top panel represents immunoblot using anti-GFP antibody and the bottom panel represents the corresponding gel stained using Coomassie. **(B)** Leaf conductance time courses (n=3 leaves per genotype) in response to changing ambient $CO_2$ which is 400 ppm for the first 10 minutes, raised to 1000 ppm for one hour and brought back to 400 ppm for another hour. Note the unresponsiveness for both the *tpk1* and *kin7* loss of function mutants.

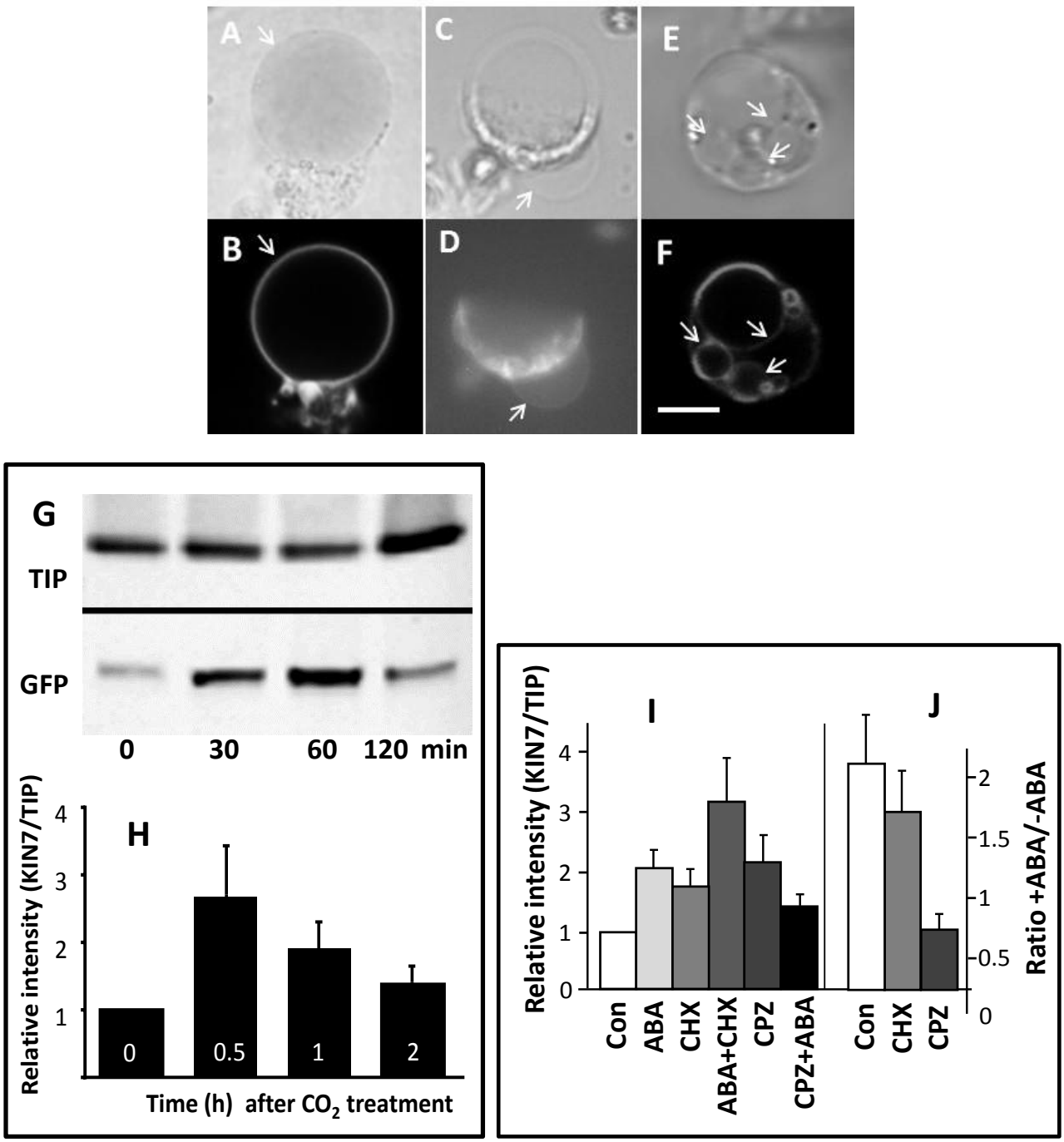


**Figure S4: KIN7-YFP membrane expression pattern, $CO_2$ induced shift in expression and the effect of protein synthesis and endocytosis inhibitors (relating to Figure 3).** **(A, B)** Arabidopsis guard cells transiently transformed with 35S:KIN7-YFP show KIN7 expression in tonoplast (white arrows). **(C, D)** Partially disrupted guard cell protoplast transiently transformed with Kin7p:KIN7-YFP shows fluorescence in large vacuolar bulge (arrows). **(E, F),** Guard cell protoplasts isolated from plants stably transformed with Kin7p:KIN7-YFP shows fluorescence large and multiple small vacuoles (arrows).Top row shows DIC images, bottom row shows corresponding epifluorescence images. Scale bar is 3 µm. **(G)** Example Western blot using antibodies against KIN7-GFP and TIP1;1, showing that $CO_2$ treatment (1000 ppm, 3h) causes an increase in KIN7 expression relative to TIP1;1, a marker for the tonoplast. **(H)** Data were quantified on the basis of 3 independent biological replicates, error bars denote standard errors. **(I)** Treatment of plants with ABA,

cycloheximide (CHX, a protein synthesis inhibitor) or chlorpromazine (CPZ, an inhibitor of endocytosis) on their own, causes a shift in KIN7 expression towards tonoplast location. Cycloheximide and chlorpromazine stimulate an increased KIN7:TIP ratio when used on their own, pointing to non-specific effects of these inhibitors. The effect of ABA is abrogated in plants pre-treated with chlorpromazine. This becomes obvious when plus/minus ABA ratios are compared for the various treatments (Figure 3B). **(J)** Same data as in (A) but expressed as a ratio of plus ABA to minus ABA treatment. This shows that cycloheximide does not affect the ABA-dependent shift toward tonoplast expression whereas chlorpromazine strongly inhibits it. Data are from 3 independent experiments and error bars denote standard errors.

| KIN# | Gene ID | Annotation | Mutant line | TMD |
|---|---|---|---|---|
| 1 | AT1G21250 | WAK1, wall associated kinase | SALK_209668 | 1 |
| 2 | AT1G48480 | RKL1 (Receptor-like kinase 1) | SALK_099094 | 2 |
| 3 | AT1G51805 | Leucine-rich repeat protein kinase, | SALK_003231 | 1 |
| 4 | AT1G53730 | SRF6 (Strubbelig-receptor family 6) | SALK_054337 | 2 |
| 5 | AT1G66150 | TMK1 (Transmembrane kinase 1) | SALK_008771 | 1 |
| 6 | AT2G26730 | Leucine-rich repeat transmembrane protein kinase | SALK_034004 | 1 |
| 7 | AT3G02880 | Leucine-rich repeat transmembrane protein kinase | SALK_019840/FLAG_321B08 | 1 |
| 8 | AT3G14840 | Leucine-rich repeat family protein | SALK_094512 | 2 |
| 9 | AT3G22060 | Receptor protein kinase-related | SALK_151902 | 1 |
| 10 | AT4G01330 | Protein kinase family protein | SALK_081284 | 1 |
| 11 | AT4G21380 | ARK3 (*Arabidopsis* Receptor Kinase 3) | SALK_001986 | 2 |
| 12 | AT4G21410 | Protein kinase family protein (CRK29) | SAIL_447_F06 | 1 |
| 13 | AT4G29130 | AtHXK1 (GLUCOSE INSENSITIVE 2) hexokinase | SALK_018086 | 1 |
| 14 | AT4G34220 | Leucine-rich repeat transmembrane protein kinase | SALK_112336 | 2 |
| 15 | AT5G38990 | Protein kinase family protein | SALK_139579 | 1 |
| 16 | AT5G49760 | Leucine-rich repeat family protein kinase | SALK_118908 | 2 |

**Table S1: Vacuolar kinases (related to Figure 1, Table S2 and Figure S2).**
Membrane kinases identified in the SUBA database (suba2.plantenergy.uwa.edu.au/) with a 'vacuolar' localisation based on either 'GFP' or MS/MS analyses. 'TMD': putative number of transmembrane domains. For each, loss of function mutants were obtained which were genotyped using T-DNA and gene specific primers (see Table S2). RT-PCR on RNA from homozygous lines was carried out, using gene specific primers, to ensure no transcript was present.

| Mutant Line | Forward and Reverse genotyping primers |
|---|---|
| SALK_209668 | 5'AATCTGCGAAATGTCATGAGG3'<br>5'TTGGTATCAGCCTTGAAGCAC3' |
| SALK_099094 | 5'TCTCTGTTTTCCTCTCCCTCC3'<br>5'GTCAAGCACTGCCTTATACGC3' |
| SALK_003231 | 5'TTCTTACATGACAAAAATTCAGGG3'<br>5'AGCTCAAGATCAACCCGGTAC3' |
| SALK_054337 | 5'AACGACTTTCACGGTATGCAC3'<br>5'TGTCAAATGGTTTTCTCCCAG3' |
| SALK_008771 | 5'CGAGAAAACCGGGTAAAGAAC3'<br>5'TTTTTGTGCGAATAAACAACTTG3' |
| SALK_034004 | 5'GCCCACCAGATAAATATTTGC3'<br>5'AGTGAGTCGACCTAAGGAGCC3' |
| SALK_019840 | 5'CATGAAAACAAAGGGATGAGG3'<br>5'CACGCAGAGGATATCGAGAAG3' |
| GABI_047F11 | 5'TAAATGGTTTAAGCGGTGTGC3'<br>5'ATCAGCAACGGACATTTCAAC3' |
| FLAG_321B08 | 5'TATTCCGAGTTCGTTGTCGTC3'<br>5'GGAAACGGGAGAACTCCGTT3' |
| SALK_094512 | 5'CATCGATCATGCCATAAATCC3'<br>5'GAGCAGTTACAAGTAACGGCG3' |
| SALK_151902 | 5'TTTACCGTCGCAACAGTTAGG3'<br>5'TTAAAACGCATCGTTTGGTTC3' |
| SALK_081284 | 5'TTCGTCTCGATATGGACAAGG3'<br>5'GACGACCCAAAGCTTTAGACC3' |
| SALK_001986 | 5'TCAAAGACATCAGTTCAGGGG3'<br>5'TTCACTGTCCATGATTCATCG3' |
| SAIL_447F06 | 5'TCTCAGCATCACAACAACTCG3'<br>5'AAATACAGCAGGAGGGATGTG3' |
| SALK_018086 | 5'CTCGAAACTGAGACAAGTGGC3'<br>5'GTCTTCGCATTCTGTAGCGAC3' |
| SALK_112336 | 5'CTCGAAACTGAGACAAGTGGC3'<br>5'GTCTTCGCATTCTGTAGCGAC3' |
| SALK_139579 | 5'CTCTCGAATTCCTTGGGTTTC3'<br>5'CAATCTCTCTGGTGATTTGCC3' |
| SALK_118908 | 5'TCAATGGACGTAACTTTGAGG3'<br>5'AGTGAAACGGTTGACGTTGAC3' |
| | Cloning primers |
| kin8bifcfwd | CCACTAGTGGAACAATGTCGTTAAATCGACAACTTCT |
| kin8bifcrev | CGACTCGAGAGTTCTAGTGTTCCAATAGG |
| kin12bifcfwd | CCGGATCCGGAACAATGGAACATGTCAGAGTTATCT |
| kin12bifcrev | CGACTCGAGACGAGGAGAAAACTCAGAAA |
| kin7bifcfwd | CCACTAGTGGAACAATGAAGTATAAGCGTAAGCT |
| kin7bifcrev | CGACTCGAGGTCGGATACAGGATTTGGGG |
| tpk1bamhIf | GGATCCATGTCGAGTGATGCAGCT |
| tpk1xhoir | CTCGAGCTACATGATCACTCGCCTGAG |
| kin7yfpfwd | CGACTCGAGAACAATGAAGTATAAGCGTAAGCT |
| promkin7fwd | ATGTCTTTGGTCACACTCAACCTGC |
| promkin7rev | CACTCGAGCTTCTTCTTCTTCTTCAAAAAC |
| kin7yfpfwd | CGACTCGAGAACAATGAAGTATAAGCGTAAGCT |
| kin7yfprev | ACCCGGGGTCGGATACAGGATTTGGGG |

**Table S2: Genotyping and cloning primers (related to Star Method section 'Plants' and 'Cloning of kinases in the BiFC vector').**

Gene specific primers used to identify homozygous lines for kinase mutant lines listed in Table S1 and cloning primers used to make kinase-YFP fusion proteins.